Electrical Power and Energy Systems 44 (2013) 388–402

Contents lists available at SciVerse ScienceDirect

Electrical Power and Energy Systems

journal homepage: www.elsevier.com/locate/ijepes

Primary frequency control of multi-machine power systems with STATCOM-SMES: A case study

Marcelo G. Molina *, Pedro E. Mercado

CONICET, Instituto de Energía Eléctrica (IEE), Universidad Nacional de San Juan (UNSJ), Av. Libertador San Martín Oeste, 1109, J5400ARL San Juan, Argentina

ARTICLE INFO

Article history:
Received 6 February 2008
Received in revised form 30 September 2011
Accepted 10 October 2011

Keywords:
Primary frequency control
FACTS
STATCOM
Superconducting magnetic energy storage (SMES)
Detailed model
Simplified model

ABSTRACT

Primary frequency control (PFC) has the ability to regulate short period random variations of frequency during normal operation conditions and response to emergency rapidly. However, in the last decade, many large blackouts happened worldwide that led to serious economic losses. It allows concluding that the ability of current PFC to meet an emergency is poor, and security of power system (PS) should be improved. An alternative to effectively enhance the PFC and thus the PS security is to store exceeding energy during off-peak load periods in efficient energy storage systems (ESSs) for substituting the primary control reserve. In this sense, superconducting magnetic energy storage (SMES) in combination with a Static Synchronous Compensator (STATCOM) are capable of supplying power systems with both active and reactive powers simultaneously and very fast, and thus to enhance the system security dramatically. In this paper, a new concept of PFC based on incorporating a STATCOM coupled with a SMES device is presented. A full detailed model of the integrated STATCOM-SMES is proposed, including a pseudo 48-pulse voltage source inverter (VSI) and a two-quadrant three-level dc–dc converter as interface with the SMES. In addition, a dynamic equivalent model of the STATCOM-SMES for multi-machine power system studies is presented. The proposed simplified modeling is developed using the state-space averaging technique and is implemented in the MATLAB/Simulink environment using the phasor simulation method. Moreover, a three-level control scheme is designed, including a full decoupled current control strategy in the d–q reference frame with a novel controller to prevent the STATCOM dc bus capacitors voltage imbalance and an enhanced power system frequency controller.

1. Introduction

Power system (PS) security is, jointly with economy, the most important requirement during the operation of the electric system. This is related to the system capability of maintaining operational in case of an unexpected failure of any of its components [1]. From this, the necessity emerges of having available enough short-term generation reserve in order to preserve adequate security levels. This reserve must be appropriately activated by means of the primary frequency control (PFC) [2]. In this way, the system frequency can be kept within acceptable limits all the time independently of any disturbance. PFC is one of the key means in order to ensure PS security and stability. It can regulate short period random variations of frequency during normal operation conditions and response to emergency rapidly [3]. However, in the last decade, many large blackouts happened worldwide that led to serious economic losses. It allows concluding that the ability of current PFC to meet an emergency is poor, and security of power system should be improved [4,5]. In fact, this situation has become worse in the last years with the deregulation of the electricity market, which has given rise to many opportunities to interconnect local and regional systems. With these additional electrical links were introduced new electromechanical oscillation modes between electrically coherent power plants or areas. As a result, new deregulated markets with high competitiveness impose greater challenges to power systems, as they can no longer be operated in a structured, conservative manner [6]. The significant structural changes and complex ownership issues associated with this new environment demand for improved approaches to PS security. The efficient use of the electric systems while maintaining security levels requires more sophisticated control schemes using advanced technologies [7].

An alternative to effectively enhance the PFC and thus the PS security is to store exceeding energy during off-peak load periods in efficient energy storage systems (ESSs) for substituting the primary control reserve. In this sense, modern ESS in combination with flexible ac transmission systems (FACTSs) are capable of supplying power systems with both active and reactive powers simultaneously and very fast, and thus capable of enhancing the systems security dramatically [8].

* Corresponding author. Tel.: +54 264 4226444; fax: +54 264 4210299.
E-mail address: mgmolina@iee.unsj.edu.ar (M.G. Molina).

0142-0615/$ - see front matter © 2012 Elsevier Ltd. All rights reserved.
http://dx.doi.org/10.1016/j.ijepes.2011.10.035

In recent years, it has been gradually seen that ESS advanced solutions such as superconducting magnetic energy storage (SMES) have received significant interest for high power utility applications [8,9]. The rapid advances in superconductive technology have permitted such devices of reasonable size to be designed and commissioned successfully. In this way, main features of SMES coils, such as rapid response (ms), high power (hundred MW), high efficiency, and four-quadrant control can be effectively used in order to store excess energy for substituting the generation reserve during the action of the PFC. By combining the technology of superconduction with a recent type of power electronic equipments, such as static converter-based FACTS controllers [10–12], the PS can take advantage of the flexibility benefits provided by SMES coils and the high controllability provided by power electronics aiming at controlling and optimizing the performance of the electric system. A previous study of the dynamic performance of converter-based FACTS devices jointly with SMES units has suggested the use of a Static Synchronous Compensator controller (STATCOM) as the most adequate for PFC applications [12].

This paper presents a novel PFC scheme based on incorporating a STATCOM controller coupled with a SMES device. A full detailed model of the integrated STATCOM-SMES controller is proposed, including a pseudo 48-pulse voltage source inverter (VSI) with phase control, and a two-quadrant PWM three-level dc–dc converter as interface between the STATCOM and the SMES. In addition, a dynamic equivalent model of the STATCOM-SMES for multi-machine power system studies is presented. The proposed simplified modeling is developed using the state-space averaging technique and is implemented in the MATLAB/Simulink environment using the phasor simulation method. Moreover, a three-level control scheme is designed, including a full decoupled current control strategy in the d–q reference frame with a novel controller to prevent the STATCOM dc bus capacitors voltage drift/imbalance and an enhanced power system frequency controller. The dynamic performance of the presented developments is evaluated through computer simulations, using a simple test power system for the case of the detailed modeling approach and a real multi-machine power system such as the Argentinean high voltage interconnected power system for the case of the simplified modeling methodology.

2. Detailed modeling of the proposed STATCOM-SMES controller

Fig. 1 summarizes the proposed detailed model of the STATCOM-SMES controller for dynamic performance studies in high power systems [12,13]. This model consists mainly of the STATCOM controller, the SMES coil with the corresponding filtering and protection system and the interface between the STATCOM and the SMES, represented by the dc–dc converter.

2.1. Three-level 48-pulse VSI-based STATCOM

The STATCOM basically consists of a voltage source inverter with semiconductors devices having turn-off capabilities, step-up transformers and dc bus capacitors. The VSI depicted in Fig. 1 (middle side, into the STATCOM) corresponds to a dc to ac switching power converter using GTO thyristors in appropriate circuit configurations in order to generate a balanced set of three sinusoidal voltages at the fundamental frequency. A line-frequency switching modulation method with selective harmonics elimination in order to build the pseudo 48-pulse inverter is proposed here for high power applications. This phase control scheme involves multi-connected, elementary three-level inverters in an appropriate multi-pulse arrangement. The VSI structure makes use of a three-level structure, also known as neutral point clamped (NPC) multi-level inverter, instead of a standard two-level 6-pulse structure. The topology used attempts to address some of the limitations of the standard two-level inverter such as the difficulty to extend the power capability of the inverter beyond the ratings of an individual switching device and the need of PWM or pulse-dropping techniques to improve the poor harmonic performance of the inverter [14]. The three-level structure offers the additional flexibility of a

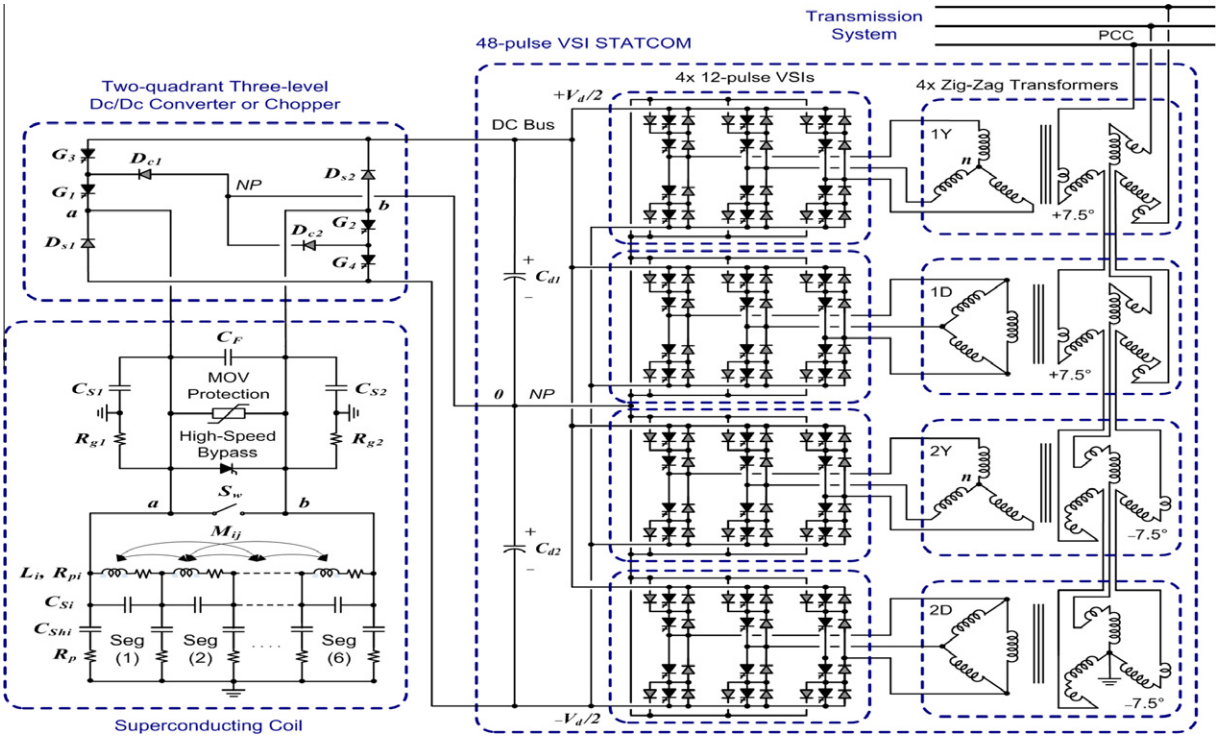

Fig. 1. Detailed model of the proposed STATCOM-SMES controller.

level in the output voltage, which can be controlled in duration, either to vary the fundamental output voltage, or to assist in the output waveform construction as is used in this work.

The elementary three-level 6-pulse inverters can be combined so as to obtain the required multi-pulse inverter structure. Hence, by using zigzag phase-shifting transformers (PSTs) and the appropriate GTOs switching phase, the principle of harmonic neutralization can be applied. This allows reducing the harmonic level of the output voltage waveform. The connection scheme of two three-level elementary inverters (couples 1Y–1D and 2Y–2D) makes up an equivalent structure of a 12-pulse VSI. The 30° phase-shift between the primary and secondary of transformers 1D and 2D permits to cancel harmonics $5 + 12r$ (i.e., $h = 5, 17, 29, 41, \ldots$) and $7 + 12r$ $(7, 19, 31, 43, \ldots)$, where $r = 0, 1, 2, \ldots$. In the same way, by combining two three-level 12-pulse VSIs, phase-shifted 7.5° from each other, an equivalent 24-pulse inverter is build. This structure is able to behave like an equivalent standard two-level 48-pulse inverter for an optimum setting of β, during which the elementary VSI output voltage is zero. The 15° phase shift between the two groups of transformers (1Y–1D leading by 7.5° and 2Y–2D lagging by 7.5°) allows cancellation of harmonics $11 + 24r$ $(11, 35, \ldots)$ and $13 + 24r$ $(13, 37, \ldots)$. As all $3r$ harmonics are not transmitted by the Y and D transformers secondaries, the first harmonics which are not cancelled by the transformers are 23rd, 25th, 47th and 49th. By choosing an appropriate value for β, that is $\beta_{optimum} = 3.75°$, the 23rd and 25th harmonics of the equivalent 24-pulse inverter can be minimized, as can be observed from harmonic content shown in Fig. 2a. In this way, the first significant harmonics are the 47th and 49th, the inverter acting as an equivalent standard 48-pulse VSI. This topology permits to generate an almost sinusoidal voltage waveform consisting of 48 steps, as shown in Fig. 2b for a capacitive operation mode. The voltage THD with this topology is lower than 3%; consequently this VSI can be used in high power applications without ac filters. Even more, this controller supplies at the point of common coupling (PCC) to the electric grid an almost sinusoidal current; the current being smoothed by the leakage inductance of the step-up coupling transformers which act as a natural low-pass filter.

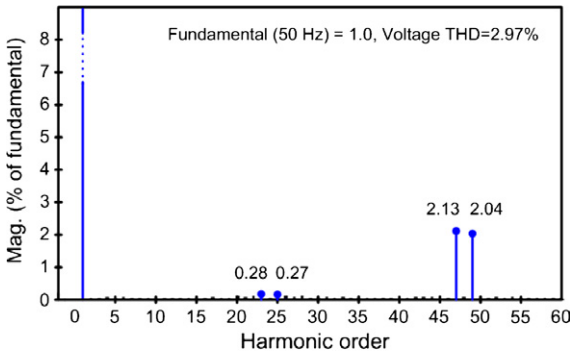

(a) Voltage harmonic content

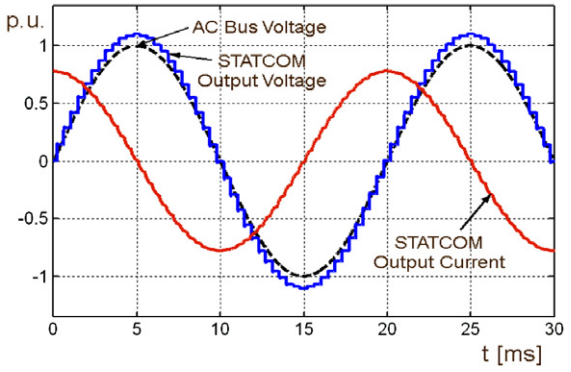

(b) Voltage and current output waveforms

Fig. 2. Equivalent 48-pulse VSI-based STATCOM voltage THD and output waveforms for optimum conduction angle operation.

The mathematical equations describing the operation of the pseudo 48-pulse VSI proposed can be derived from the detailed model shown in Fig. 1 by taking into account some assumptions respect to the operating conditions of the inverter. For this purpose, a simplified scheme of the VSI connected to the electric system is employed, also referred to as an averaged model, as depicted in Fig. 3. The static inverter operation under balanced conditions is considered as ideal, i.e. the VSI is seen as an ideal sinusoidal voltage source operating at fundamental frequency. This consideration is valid since the harmonics generated by the inverter as result of the 48-pulse control technique employed are low enough, as was verified from Fig. 2b, and the net instantaneous output voltages at the PCC resembles three sinusoidal waveforms phase-shifted 120° between each other.

The equivalent ideal inverter depicted in Fig. 3 is shunt-connected to the ac network through the inductance L_S, accounting for the equivalent leakage of the four actual step-up transformers and the series resistance R_S, representing the transformer winding resistance and VSI semiconductors conduction losses. The magnetizing inductance of the actual step-up transformers is also taken in consideration through the mutual equivalent inductance M. In the dc side, the equivalent capacitance of the two dc bus capacitors, C_{d1} and C_{d2} ($C_{d1} = C_{d2}$), is described through $C = C_{d1}/2 = C_{d2}/2$ whereas the switching losses of the VSI and power loss in the dc capacitors are considered by R_p.

The dynamics equations governing the instantaneous values of the three-phase output voltages in the ac side of the VSI and the

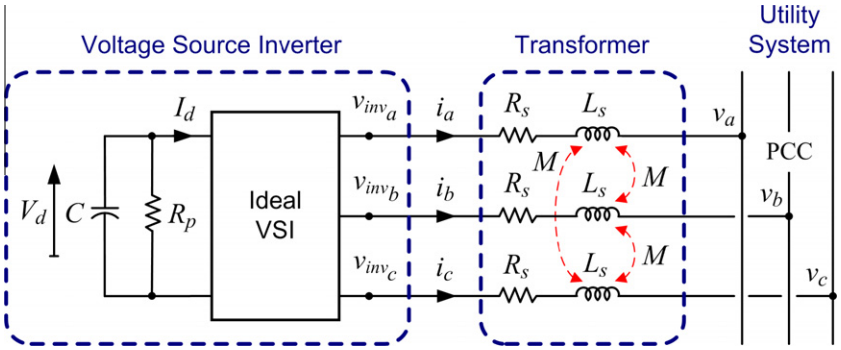

Fig. 3. Equivalent circuit diagram of the proposed pseudo 48-pulse VSI connected to the ac system.

current exchanged with the electric network can be directly derived from Fig. 3 by applying Kirchhoff's voltage law (KVL) [13] as follows:

$$\begin{bmatrix} v_{inv_a} \\ v_{inv_b} \\ v_{inv_c} \end{bmatrix} - \begin{bmatrix} v_a \\ v_b \\ v_c \end{bmatrix} = (\mathrm{R_s} + s\mathrm{L_s}) \begin{bmatrix} i_a \\ i_b \\ i_c \end{bmatrix}, \tag{1}$$

where

$$s = \frac{d}{dt} \quad \mathrm{R_s} = \begin{bmatrix} R_s & 0 & 0 \\ 0 & R_s & 0 \\ 0 & 0 & R_s \end{bmatrix}, \quad \mathrm{L_s} = \begin{bmatrix} L_s & M & M \\ M & L_s & M \\ M & M & L_s \end{bmatrix}. \tag{2}$$

Under the assumption that the system has no zero sequence components (operation under balanced conditions), all currents and voltages can be uniquely transformed into the synchronous-rotating orthogonal two-axes reference frame, in which each vector is described by means of its d and q components, instead of its three a, b, c components. Thus, as shown in Fig. 4, the new coordinate system is defined with the d-axis always coincident with the instantaneous voltage vector. By defining the d-axis to be always coincident with the instantaneous voltage vector v, yields v_d equals $|v|$, while v_q is set at zero. Consequently, the d-axis current component contributes to the instantaneous active power and the q-axis current component represents the instantaneous reactive power. This operation permits to develop a simpler and more accurate dynamic model of the VSI.

By applying Park's transformation and neglecting the zero sequence components, Eqs. (1) and (2) can be transformed into the synchronous rotating d–q reference frame as follows:

$$\begin{bmatrix} v_{inv_d} \\ v_{inv_q} \end{bmatrix} - \begin{bmatrix} v_d \\ v_q \end{bmatrix} = (R_s + sL'_s) \begin{bmatrix} i_d \\ i_q \end{bmatrix} + \begin{bmatrix} -\omega & 0 \\ 0 & \omega \end{bmatrix} L'_s \begin{bmatrix} i_q \\ i_d \end{bmatrix}, \tag{3}$$

where

$$R_s = \begin{bmatrix} R_s & 0 \\ 0 & R_s \end{bmatrix}, \quad L'_s = \begin{bmatrix} L'_s & 0 \\ 0 & L_s \end{bmatrix} = \begin{bmatrix} L_s - M & 0 \\ 0 & L_s - M \end{bmatrix}. \tag{4}$$

It is to be noted that the coupling of phases a–b–c through the term M in matrix L_s (Eq. (2)), was fully eliminated in the d–q reference frame when the VSI transformers are magnetically symmetric, as is usually the case. This decoupling of phases in the synchronous-rotating system allows simplifying the control system design. A further major issue of the d–q transformation is its frequency dependence (ω). In this way, with appropriate synchronization to the network (through angle θ), the control variables in steady state are transformed into dc quantities.

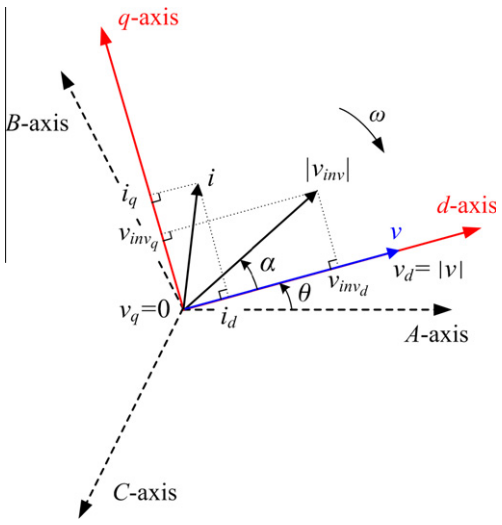

Fig. 4. VSI vectors in the synchronous rotating d–q reference frame.

The relation between the dc-side voltage V_d and the generated ac voltage v_{inv} can be described through the switching function matrix S of the equivalent 48-pulse voltage source inverter proposed, as given by Eq. (5).

$$\begin{bmatrix} v_{inv_a} \\ v_{inv_b} \\ v_{inv_c} \end{bmatrix} = \begin{bmatrix} S_a^{e48} \\ S_b^{e48} \\ S_c^{e48} \end{bmatrix} V_d. \tag{5}$$

This relation assumes that the dc capacitors voltages are balanced and equal to $V_d/2$. The switching function for the equivalent 48-pulse VSI can be estimated for phase 'a' through Eq. (6). The switching functions for phases 'b' and 'c' are similar but phase-shifted 120° and 240°, respectively.

$$S_a^{e48} \approx \sum_{h=1}^{\infty} \left[\frac{2}{h\pi} k_T \cos(h\beta) \sin(h\omega t) \right], \tag{6}$$

being $h = 48m \pm 1$ any positive integer, that is, $h = 1, 47, 49, \ldots$ for all $m = 0, 1, 2, \ldots$, $k_T = 4\frac{n_2}{n_1}$: total voltage ratio of the zigzag phase-shifting transformers, β: dead angle (period during which the elementary VSI output voltage is zero).

If the switching functions are averaged and computed in the d–q reference frame, Eq. (5) can be rewritten by using the average switching function matrix $S_{av,dq}$ of the equivalent 48-pulse VSI proposed in d–q coordinates as follows:

$$\begin{bmatrix} v_{inv_d} \\ v_{inv_q} \end{bmatrix} = S_{av,dq} V_d, \tag{7}$$

and the average switching function matrix for the dq reference frame,

$$S_{av,dq} = \begin{bmatrix} S_{av,d} \\ S_{av,q} \end{bmatrix} = \begin{bmatrix} \cos\alpha \\ \sin\alpha \end{bmatrix} S_{av}^{e48}, \tag{8}$$

being α the phase-shift of the VSI output voltage from the reference position, $S_{av}^{e48} = \frac{2}{\pi} k_T \cos\beta$: average switching function for the equivalent 48-pulse VSI.

The ac power exchanged by the VSI is related with the dc bus power on an instantaneous basis in such a way that a power balance must exist between the input and the output of static inverter. In this way, the ac power should be equal to the sum of the dc resistance power, representing losses (GTOs switching and dc capacitors) and to the charging rate of the dc capacitors:

$$\frac{3}{2}\left(v_{inv_d} i_d + v_{inv_q} i_q\right) = -\frac{C_d}{2} V_d s V_d - \frac{V_d^2}{R_p}. \tag{9}$$

Essentially, Eqs. (3)–(9) can be summarized in the state-space as described by Eq. (10). This continuous state-space averaged mathematical model describes the steady-state dynamics of the equivalent 48-pulse VSI in the dq reference frame.

$$s \begin{bmatrix} i_d \\ i_q \\ V_d \end{bmatrix} = \begin{bmatrix} \frac{-R_s}{L'_s} & \omega & \frac{S_{av,d}}{2L'_s} \\ -\omega & \frac{-R_s}{L'_s} & \frac{S_{av,q}}{2L'_s} \\ -\frac{3}{2C_d} S_{av,d} & -\frac{3}{2C_d} S_{av,q} & -\frac{2}{R_p C_d} \end{bmatrix} \begin{bmatrix} i_d \\ i_q \\ V_d \end{bmatrix} - \begin{bmatrix} \frac{|v|}{L'_s} \\ 0 \\ 0 \end{bmatrix}. \tag{10}$$

As recently reported by Molina et al. [12], modeling of static inverters by using a synchronous-rotating orthogonal d–q reference frame offer higher accuracy than employing stationary coordinates. Moreover, this operation allows designing a simpler control system than using a–b–c or α–β.

2.2. Two-quadrant three-level dc–dc converter

The inclusion of a SMES unit into the dc bus of the STATCOM demands the use of an interface to adapt the wide range of variation in voltage and current levels between both devices, especially the case of the SMES coil. Controlling the SMES coil rate of charge/discharge requires varying as much the coil voltage magnitude as the polarity according to the coil state-of-operation, while keeping essentially constant the STATCOM dc bus voltage. To this aim, a two-quadrant PWM three-level dc–dc converter or chopper is proposed to be used. This converter (top left side of Fig. 1) allows decreasing the ratings of the overall power devices by regulating the current flowing from the SMES coil to the inverter of the STATCOM and vice versa. In addition, it allows regulating the amplitude of the output voltage of the VSI, keeping constant the conduction angle σ of the inverter valves. Thus, the harmonic distortion of the STATCOM output voltage can be greatly reduced, independently of the voltage required at the PCC.

Major advantages of three-level chopper topologies compared to traditional two-level ones include reduction of voltage stress of each thyristor by half, permitting to increase the chopper power ratings while maintaining high dynamic performance. Furthermore, the proposed topology offers the availability of various redundant switching states, thus allowing generating the same output voltage vector through various states. This feature is very significant in order to reduce switching losses and dc current ripple, but mainly to prevent dc bus capacitors voltage drift/imbalance. This condition of *NP* voltage balancing is essential for avoiding contributing additional distortion to the VSI output voltage.

Table 1 lists all possible combinations of the chopper output voltage vectors, V_{ab} (defining the SMES side of the circuit as the output side) and their corresponding GTO switching states [13].

The addition of an extra level to the dc–dc chopper allows enlarging its degrees of freedom. As a result, the charge balance of the dc bus capacitors can be controlled by using the extra switching states, at the same time acting as a conventional dc–dc converter. The output voltage vectors can be selected based on the required SMES coil voltage and dc bus *NP* voltage. In this way, multiple subtopologies can be used in order to obtain output voltage vectors of magnitude 0 and $V_d/2$, in such a way that different vectors of magnitude $V_d/2$ produce opposite currents flowing from/to the neutral point. This condition causes a fluctuation in the *NP* potential which permits to maintain the charge balance of the dc-link capacitors. By properly selecting the duration of the different output voltage vectors, an efficient dc–dc controller with *NP* voltage control capabilities is obtained.

The dc–dc chopper has basically three modes of operation, namely the charge mode, the discharge mode and the stand-by mode. These modes are obtained in this work by using a buck-boost topology control mode versus bang–bang control mode, which produces higher ac losses on the SMES coil.

Table 1
Three-level chopper output voltage vectors and their corresponding GTO switching states.

States	G_1	G_2	G_3	G_4	V_{ab}
1	1	1	1	1	$+V_d$
2	0	0	0	0	$-V_d$
3	0	1	0	1	0
4	1	0	1	0	0
5	1	1	0	0	0
6	1	1	0	1	$+V_d/2$
7	1	1	1	0	$+V_d/2$
8	1	0	0	0	$-V_d/2$
9	0	1	0	0	$-V_d/2$

2.2.1. Dc–dc converter in charge mode

In the charge mode, the chopper works as a step-down or buck converter. This topology makes use of switching states 1, 5, 6 and 7, in order to produce output voltage vectors $+V_d$, 0 and $+V_d/2$ with separate contribution of charge at the *NP* from capacitors C_{d1} and C_{d2}. In this mode, thyristors G_1 and G_2 are always kept on, while thyristors G_3 and G_4 are modulated in order to obtain the appropriate output voltage, V_{ab}, across the SMES coil [12]. In this way, only subtopologies closest to the state 1 are used. In consequence, only one semiconductor device is switched per switching cycle T_s; this reducing the switching losses compared to the standard two-level converter and thus also reducing the current ripple.

The relationship between the dc–dc converter output voltage V_{ab}, and the VSI dc bus voltage V_d can be described through the switching function for the three-level chopper operating in buck mode as follows:

$$V_{ab} = S_{ch} V_d. \tag{11}$$

Fig. 5 shows the switching function of the three-level chopper operating in buck mode, which is stated in Eq. (12). It is to be noted the attribute of invariability associated to the switching states utilized for maintaining the charge balance of the dc capacitors (states 6 or 7).

$$S_{ch} = D_1 + D_2 + \sum_{h=1}^{\infty}\left[2\frac{\sin(h\,\pi D_2)}{h\pi}\cos\left[h\omega\left(t - \frac{D_2}{2f} - 2\frac{D_1}{f}\right)\right]\right] + \sum_{h=1}^{\infty}\left[\frac{\sin(2h\,\pi D_1)}{h\pi}\cos\left[h\omega\left(t - \frac{D_1}{f}\right)\right]\right], \tag{12}$$

where $h = 1, 2, 3, \ldots$, $D_1 = \frac{t_{on1}}{2T_s}$: duty cycle for either switching states 6 or 7, $D_2 = \frac{t_{on2}}{T_s}$: duty cycle for switching state 1.

2.2.2. Dc–dc converter in stand-by mode

Once completed the charging of the SMES coil, the operating mode of the converter is changed to the stand-by mode, for which only the state 5 is used. In this condition, thyristors G_3 and G_4 are switched off, while thyristors G_1 and G_2 are kept on all the time.

2.2.3. Dc–dc converter in discharge mode

In the discharge mode, the chopper operates as a step-up or boost converter jointly with the dc bus capacitors. This topology employs switching states 2, 5, 8 and 9, in order to produce at terminals *ab*, vectors $-V_d$, 0 and $-V_d/2$ with independent contribution of charge at the *NP* from capacitors C_{d1} and C_{d2}. In this mode, thyristors G_3 and G_4 are constantly kept off while thyristors G_1 and G_2 are controlled to obtain the suitable voltage V_{ab}, across the SMES coil [12]. In this way, only subtopologies closest to the state 2 are utilized.

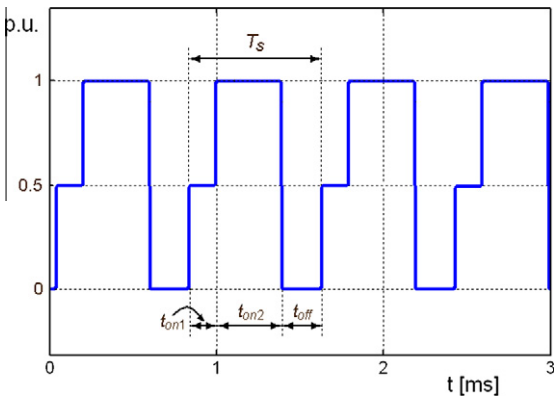

Fig. 5. Dc–dc converter switching function for charge mode.

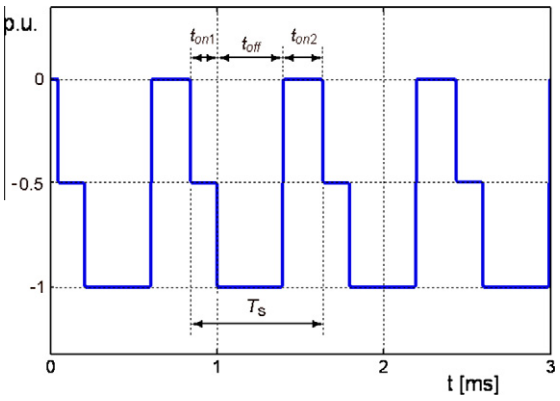

Fig. 6. Dc–dc converter switching function for discharge mode.

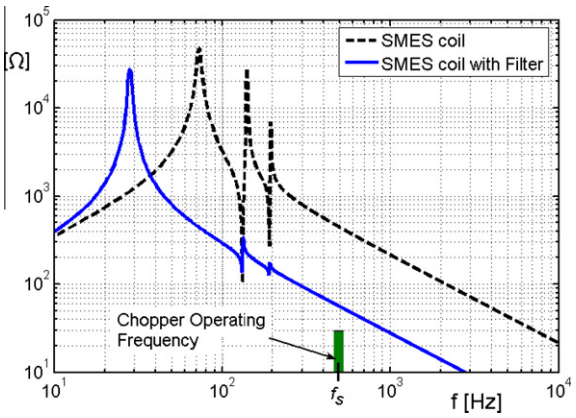

Fig. 7. SMES coil terminal impedance versus frequency with and without input filter.

As in the case of the chopper working in buck mode, the relationship between the chopper voltage V_{ab}, and the VSI dc bus voltage V_d can be derived as stated in Eq. (13):

$$V_{ab} = S_{dch}\, V_d. \tag{13}$$

Fig. 6 shows the switching function of the three-level chopper operating in discharge or boost mode. From this, the switching function expression can be derived as stated in Eq. (14). This function exhibits an analogous feature of invariability respect to the switching states utilized for generating vectors $-V_d/2$ (states 8 or 9), as in the case of the buck mode.

$$\begin{aligned} S_{dch} &= 1 - D_1 - D_2 \\ &+ \sum_{h=1}^{\infty}\left[2\frac{\sin(h\pi(1-D_2))}{h\pi}\cos\left[h\omega\left(t-\frac{(1-D_2)}{2f}-2\frac{(1-D_1)}{f}\right)\right]\right] \\ &+ \sum_{h=1}^{\infty}\left[\frac{\sin(2h\pi(1-D_1))}{h\pi}\cos\left[h\omega\left(t-\frac{(1-D_1)}{f}\right)\right]\right], \end{aligned} \tag{14}$$

where $h = 1,2,3,\ldots,$.

If the switching function is averaged it is possible to obtain a single general expression relating the chopper average output voltage V_L, to the VSI average dc bus voltage V_d. By averaging the switching functions S_{ch} and S_{dch} for both operating modes (charge and discharge), a general expression relating the chopper average output voltage V_{ab}, to the VSI average dc bus voltage V_d, can be derived:

$$V_{ab} = mV_d, \tag{15}$$

being m the modulation index expressed as: $m = (D_1 + D_2)$: chopper buck mode (charge), or: $m = -(1 - D_1 - D_2)$: chopper boost mode (discharge).

2.3. Multi-segment SMES coil

The equivalent circuit of the SMES coil depicted at the bottom left side of Fig. 1 makes use of a lumped parameters network represented by a 6-segment model comprising self inductances (L_i), mutual couplings between segments (i and j, M_{ij}), ac loss resistances (R_{si}), skin effect-related resistances (R_{pi}), turn–ground (shunt-C_{Shi}) and turn–turn capacitances (series-C_{Si}). This model is based on the one previously proposed in [15], and is reasonably accurate for electric system transients studies over a frequency range from dc to several thousand Hertz.

Fig. 7 shows the frequency domain analysis of the 6-segment SMES model, measuring the impedance of the superconducting coil across its terminals (Z_{ab}) for the case of the coil including (solid-lines) and not including (dashed-lines) surge capacitors (C_{s1} and C_{s2}) in parallel with grounding-balance resistors (R_{g1} and R_{g2}) as well as a filter capacitor C_F for reducing the effect of resonance phenomena. As can be seen from the magnitude of the terminal impedance, the coil has parallel (at around 70 Hz, 120 Hz, 200 Hz) and series (at about 110 Hz and 190 Hz) resonance frequencies. As the chopper output voltage V_{ab}, contains both even and odd harmonics of the switching frequency, coil resonances may be excited which may cause significant voltage amplification with the consequent addition of insulation stress within the coil. Since the SMES coil has a rather high inductance, these resonance frequencies become lower, turning this phenomena an issue for selecting the chopper operating frequency. Moreover, high power dc–dc converters utilize low operating frequencies in order to minimize losses, being significant in consequence to take into consideration the coil resonance phenomena for choosing a safety frequency band of operation for the chopper. In this work the switching frequency of the chopper is set at 500 Hz, minimizing the appearance of resonance effects and switching losses.

3. Simplified dynamic modeling of the proposed STATCOM-SMES controller

The equivalent dynamic modeling of the proposed STATCOM-SMES controller is carried out through the implementation of Eqs. (1)–(16) in the MATLAB environment [16], as depicted in Fig. 8. Since the required STATCOM-SMES controller in this case study is very large, a STATCOM-SMES arrangement composed of 10 individual 100 Mvar-100 MW/1000 MJ STATCOM-SMES devices conveniently disposed is considered. This group of controllers is modeled through an aggregated model approach represented using a single power electronics device with an n_c number of identical SMES coils linked to the dc bus. This approach neglects the mutual interaction between the superconducting coils but is valid for most power systems studies.

Since the multi-machine power system to be used in this case study largely increases complexity by adding extra lines, loads, transformers, and machines when compared with the previous test system, the required simulation time with the discretization of the electrical system would become prohibitive. Moreover, as the interest of the study is in slow electromechanical oscillation modes then several tens of seconds in simulation would imply computing times of even hours. In this way, conventional continuous or discrete solution methods are not practical for stability studies involving low-frequency oscillation modes. Such studies are able to be performed in Simulink through the phasor simulation method. In the phasor solution method, the fast modes of oscillations are ig-

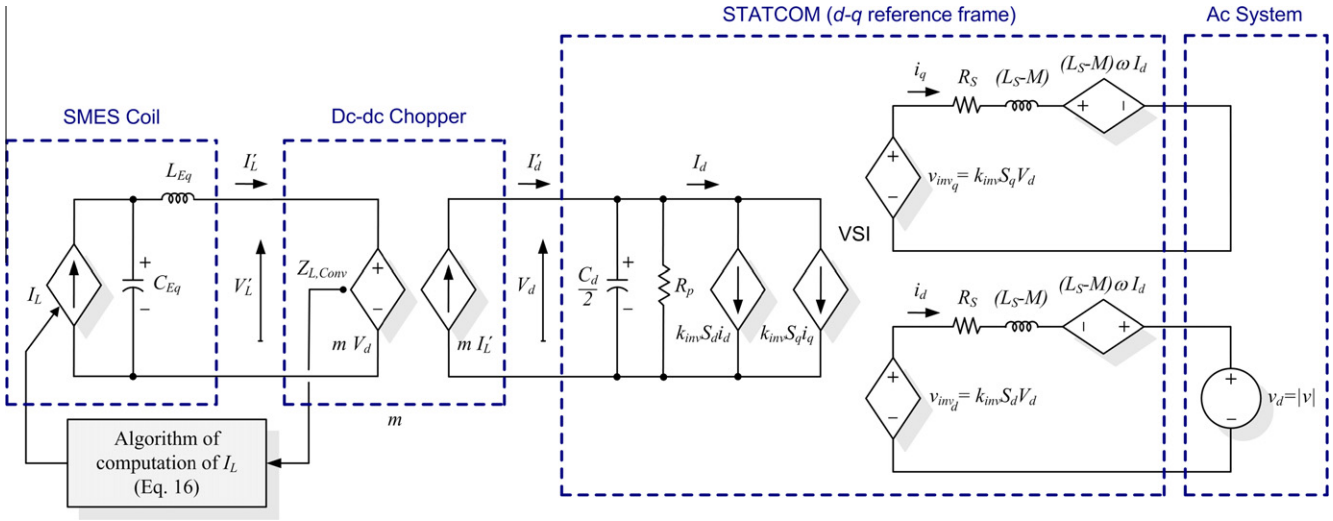

Fig. 8. Simplified dynamic model of the STATCOM-SMES controller.

nored by replacing the electric system differential equations by a set of algebraic equations. The state-space model of the network is therefore replaced by a transfer function evaluated at the fundamental frequency. The phasor solution method uses a reduced state-space model at the frequency *f*, consisting of slow states of machines, turbines, and regulators, thus dramatically reducing the required simulation time.

The detailed multi-segment representation of the SMES coil can be reduced in this simplified case study to an equivalent SMES inductor representation with stray capacitance (C_{Eq}) and inductor (L_{Eq}), as shown in Fig. 8 (left side). This equivalent model is valid only as an average means and does not consider the interaction between the SMES coil and the dc–dc chopper from the point of view of the harmonics and natural resonances. Exploring the SMES coil behavior, it can be observed that the coil representation can be described by a controlled dc current source. The charge/discharge profile of the SMES system needs be included in this model by calculating the magnitude of the actual current I_L of the superconducting coil at all times. With this aim in mind, an algorithm is proposed for the computation of I_L, which is stated in Eq. (16).

$$I_L = I_{L0} e^{-\frac{1}{L_{Eq}} \int_{t_0}^{t} Z_{L,Conv} dt}, \tag{16}$$

where I_L is the current of the SMES coil at time *t*, I_{L0} the initial current of the SMES coil (according to the initial state of charge), L_{Eq} the equivalent inductance of the SMES coil, accounting for self inductances L_i of the detailed six-segment model, $Z_{L,Conv}$ the equivalent impedance of the chopper input at time *t*, calculated constantly as follows:

$$Z_{L,Conv} = \frac{mV_d}{I'_L}. \tag{17}$$

4. Novel three-level control scheme of the STATCOM-SMES

The novel three-level control scheme of the proposed STATCOM-SMES device is designed from the steady-state average model developed in Section 2. This hierarchical control system, consisting of an external, middle and internal level, is based on concepts of

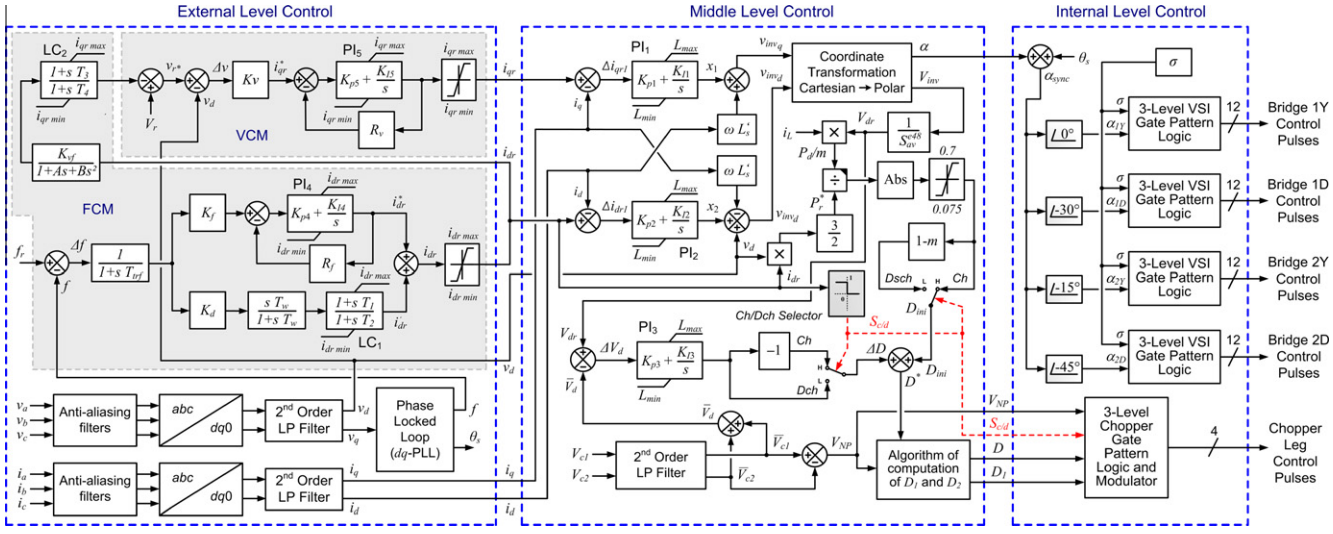

Fig. 9. Proposed three-level control scheme of the STATCOM-SMES system.

instantaneous power on the synchronous-rotating d–q reference frame, as depicted in Fig. 9.

4.1. External level control design

The proposed external level control, which is outlined in Fig. 9 (left side), is responsible for determining the active and reactive power exchange between the STATCOM-SMES device and the utility system. This control strategy is designed for performing two major objectives (control modes) with dissimilar priorities.

- Frequency control mode (FCM). Case of a STATCOM-SMES controller with active and reactive power exchange capabilities.
- Voltage control mode (VCM). Case of a traditional STATCOM with only reactive power compensation capabilities.

4.1.1. Frequency control mode

This highest-priority control mode accomplished by the upper blocks of the external level aims at controlling the PS frequency through the modulation of both, the reactive component of the output current i_q (case of a conventional STATCOM) and the active component i_d (case of a STATCOM-SMES). In the case of controlling i_q, the set-point of the VCM, i.e. the voltage reference signal V_r, is varied with a stabilizer voltage signal proportional to Δf (defined as f_r–f) which directly represents the power oscillation of the PS. This added signal causes the output quadrature current of the STATCOM, i_q to vary around the operating point defined by V_r, the purpose of this variation being to improve the damping of the power oscillations. In this way, the voltage at the PCC is forced to decrease when the frequency deviation Δf is positive aiming at reducing the transmitted power through the transmission system and thus providing an effective fast-acting voltage reduction reserve which opposes the deceleration of generators in the PS. This action is performed in the opposite way when the frequency deviation Δf is negative, and then generators accelerate. Two transfer functions, including a lag-compensator, are used to assist in shaping the gain and phase characteristics of the frequency stabilizer for the case of modulating the output quadrature current of the STATCOM.

Although the power oscillation damping approach of the standard STATCOM is rather effective, the most effective compensation action for power oscillations (or swings) damping and thus for PFC is carried out by rapidly exchanging active power with the utility system, that is to say by controlling the output direct current of the STATCOM-SMES, i_d. Considering this case, as in the previous case, the reference of the STATCOM-SMES output direct current is directly derived from Δf, representing the power oscillation of the system. The frequency transducer transfer function is designed to eliminate any dc component that may be present on the signal Δf, by proper setting of the constant T_{trf} of the low-pass filter. Since a robust and efficient frequency control scheme requires the effective damping of a wide range of generators power oscillations, ranging from less than 0.2 Hz for global oscillations to 4 Hz for local oscillations of units, a decoupled two-loop control approach with differential bands of damping is proposed in this work. Thus, a loop is dedicated to low and intermediate frequency modes of oscillations while the other one covers the high frequency mode.

The first loop is composed of a proportional–integral (PI) controller (PI_4) with output restriction including an anti-windup system to enhance the dynamic performance of the PFC system. A speed-droop R_f (typically 3%) is also included in order to obtain a stable load division among several fast-response devices operating in parallel. This characteristic is analogous to the one included in generators speed governors. Thus, the rapid active power exchange between the STATCOM-SMES and the PS is controlled, forcing the SMES coil to absorb active power when generators accelerate (charge mode), or to inject active power when they decelerate (discharge mode). The PI controller including a droop feedback acts as an overall first-order lag-compensator. This first loop ensures an excellent performance in damping power oscillations at low and intermediate frequency modes and then for large-signal stability, but its response is very poor for the high frequency mode. To this end, a supplementary signal proportional to the rate of change of the system frequency has been included via the second loop in order to speed-up the transient response of the controller for managing high frequency modes of oscillations. A differential signal of the frequency error with restricted high frequency gain is obtained by using a first-order washout filter. A lag-compensator is also included into the loop in order to improve the dynamic response of the controller and to ensure the robust global damping provided by the proposed PFC mode. This second loop provides an excellent performance in damping power oscillations at high frequency modes and then for small-signal stability. Therefore, both loops act independently, so that their effects add up to provide effective damping of all modes of interest. In this way steady state and transient objectives are fulfilled by this control strategy almost uniformly. The stabilizer signal composed from both loops is passed through a final limiter for setting the reference i_{dr}.

In all cases, the frequency signal is derived from the positive sequence components of the ac voltage vector measured at the PCC of the STATCOM-SMES, through a phase locked loop (PLL). The design of the PLL is based on concepts of instantaneous power theory in the dq reference frame. This device also synchronizes, by providing the phase θ, the coordinate transformations from abc to dq components in the voltage and current measurement system [17]. These signals are then filtered by using second-order low-pass filters in order to obtain the fundamental components employed in the control system.

4.1.2. Voltage control mode

This subordinate control mode has the goal of controlling (supporting and regulating) the voltage at the PCC to the electric grid. It has proved very good performance in conventional STATCOM controllers through the modulation of the reactive component of the output current i_{qr}. To this end, in this work the instantaneous voltage at the PCC is computed by using a synchronous-rotating reference frame. In consequence, by applying Park's transformation, the instantaneous values of the three-phase ac bus voltages are transformed into d–q components, v_d and v_q respectively. By defining the d-axis always coincident with the instantaneous voltage vector v, then v_d results equal to $|v|$ while v_q is set at zero, as can be derived from Fig. 4. Consequently, only v_d is used for computing the voltage error vector which is introduced to a proportional–integral (PI) controller with output restriction including an anti-windup system to enhance the dynamic performance of the VCM system. A voltage regulation droop R_d (typically 5%) is included in order to allow a higher operation stability of the STATCOM-SMES device in cases that more high-speed voltage compensators are operating in the area. This characteristic is comparable to the one included in generators voltage regulators. As a result, the PI controller including a droop feedback acts as an overall first-order lag-compensator.

4.2. Middle level control design

The middle level control makes the expected output, particularly the actual active and reactive power exchange between the STATCOM-SMES and the ac system, to dinamically track the reference values set by the external level. The middle level control design, which is depicted in Fig. 9 (middle side), is based on a linearization of the simplified state-space averaged mathematical

model of the STATCOM-SMES controller in the d–q reference frame, described in Section 2.

In order to achieve a decoupled active and reactive power control, it is required to provide a full decoupled current control strategy for i_d and i_q. Inspection of Eq. (10) shows a cross-coupling of both components of the STATCOM-SMES controller output current through ω. Therefore, in order to decouple the control of i_d and i_q, appropriate control signals have to be used. Thus, by generating the control signals x_1 and x_2 derived from setting to zero the derivatives of currents in the upper part (ac side) of Eq. (10), the middle level control algorithms are obtained. In order to achieve this condition in steady-state, two conventional PI controllers with proper feedback of the STATCOM-SMES output current components are introduced, yielding Eq. (18) as follows:

$$s\begin{bmatrix} i_d \\ i_q \end{bmatrix} = \begin{bmatrix} \frac{-R_s}{L'_s} & 0 \\ 0 & \frac{-R_s}{L'_s} \end{bmatrix}\begin{bmatrix} i_d \\ i_q \end{bmatrix} - \begin{bmatrix} x_1 \\ x_2 \end{bmatrix}. \tag{18}$$

As can be noticed, i_d and i_q respond to x_1 and x_2 respectively with no crosscoupling. Thus, with the introduction of these new variables this control approach allows to obtain a quite effective decoupled control with the model (ac side) reduced to first-order functions.

Fig. 9 (middle side) shows the full implementation of the middle level control. The coordinate transformation from Cartesian to Polar yields the required magnitude of the output voltage vector produced by the VSI (V_{inv}) and the phase-shift rating α of this vector from the reference position, represented by the voltage vector measured at the PCC of the STATCOM-SMES. From V_{inv}, the required voltage at the dc bus (V_{dr}) is derived and the duty cycle of the chopper thyristors (D^*) is estimated through a balance of dc power in the chopper, taking into consideration the active power injection/absorption ratings required from the STATCOM-SMES and the actual current of the SMES coil i_L. The duty cycle of the chopper GTO thyristors is then derived by relying on the mode of operation of the dc/dc chopper (charge/discharge), so that an initial value D_{ini} is determined for the thyristors duty cycle. This mode of operation is determined assessing the sign of the required positive sequence component of i_d (i_{dr1}) via a charge/discharge selection block and producing a signal of mode $S_{c/d}$ that is also required by the internal level control. A corrective action of integral-type (PI controller) is needed for an accurate tracking of the actual duty cycle D^*, being D^* the total duty ratio of the three-level chopper. Therefore, dc bus voltage deviations ΔV_d caused by actual VSC switching losses and capacitors power losses can be quickly counteracted. Finally, duty cycles D_1 and D_2 are computed from D^* through a novel controller for balancing the dc link capacitors. This novel extra dc voltage control block provides the availability of managing the redundant switching states of the chopper according to the capacitors charge unbalance measured through the neutral point voltage, $V_{PN} = \overline{V_{c1}} - \overline{V_{c2}}$. This specific loop modifying the modulating waveforms of the internal level control is also proposed for reducing instability problems caused by harmonics as much in the STATCOM-SMES device as in the electric system [18].

4.3. Internal level control design

The internal level provides dynamic control of input signals for the dc–dc and ac–dc converters. This level is responsible for generating the triggering and blocking control signals for the different valves of the pseudo 48-pulse three-level VSI and the three-level dc–dc chopper, according to the control mode (phase control) and types of valves (GTOs) used. Fig. 9 (right side) shows a basic scheme of the internal level control of the STATCOM-SMES compensator. This level is mainly composed of a line synchronization module and a firing pulses generator for both the STATCOM VSI and the dc–dc chopper. The line synchronization module simply synchronizes the STATCOM-SMES device switching pulses with the positive sequence components of the ac voltage vector at the PCC through the PLL phase signal, θ_s. In the case of the firing pulses generator block, the controller of the VSI is made up of four basic three-level 6-pulse switching generators with specific phase-shifting in order to obtain an overall 48-pulse structure. The phase-shifting between control pulses of Bridges 1Y and 1D makes an equivalent structure of a 24-pulse VSI. Hence, by lagging the control pulses of the second equivalent 24-pulse structure by 15° respect to the first, according to the phase-shifting of zigzag transformers primaries, an equivalent 48-pulse VSI is obtained. Even though the conduction angle σ can be changed to control the output voltage amplitude of the VSI, in this work the amplitude is controlled just by using the duty ratio m of the chopper. In this way, σ is kept constant at 172.5° in order to obtain the lowest voltage THD for this topology, independently of the output voltage amplitude.

5. Performance evaluation of the STATCOM-SMES modeling approach

The dynamic performance of the proposed modeling and control approach is evaluated through digital simulation carried out in the MATLAB/Simulink environment [16]. To this aim, two modeling approaches are to be used, that is a full detailed modeling and a simplified one. In the first case study, the detailed modeling is validated through a simple single-machine power system while in the second case study the simplified modeling is analyzed in a real multi-machine power system.

5.1. Case study 1: Detailed modeling evaluated in a single machine-infinite bus-type (SMIB) test system

The proposed full detailed modeling of the STATCOM-SMES controller is carried out by using SimPowerSystems (SPS) of MATLAB/Simulink. SPS (or Power System Blockset – PSB for releases preceding R13) is a modern design tool that allows to rapidly and easily building models that simulate power systems. Their libraries contain models of typical power equipment such as transformers, lines, machines, and power electronics among others. It uses the Simulink environment to interact with mechanical, thermal, control, and other disciplines. Since the proposed detailed modeling contains many states and non-linear blocks such as power electronics switches, the discretization of the electrical system with fixed-step is required so as to allow much faster simulation than using variable time-step methods [13].

The test power system used to study the detailed modeling approach is presented in Fig. 10 as a single-line diagram. This 7-bus transmission system operates at 230 kV/ 50 Hz, and implements

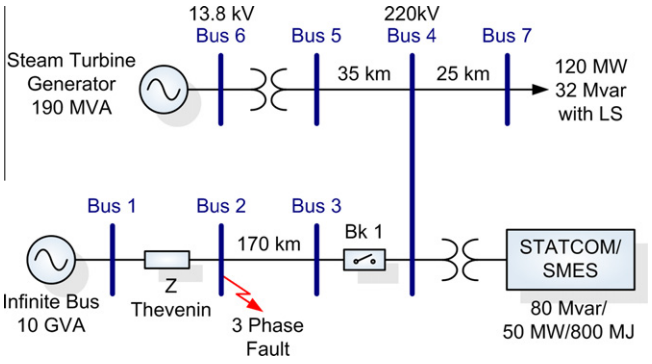

Fig. 10. Single machine-infinite bus-type (SMIB) test power system.

a dynamically-modeled single generator-type small utility linked to a bulk power system represented by a SMIB used for studies of FACTS devices [2]. The generator is powered by a steam turbine and the controls of the unit include a dc type-1a standard IEEE voltage regulator and a speed governor.

For full performance studies, a three-phase-to-ground fault is applied at bus 2 in the bulk power system at $t = 0.1$ s, and cleared 10 cycles later (200 ms) by tripping the tie line with the opening of the circuit breaker Bk 1. Two different case studies relative to basic protection rules are considered, permitting carry out a full large-signal and small-signal performance study of the STATCOM-SMES for various control modes. The first case study (Case 1.A), which corresponds to a severe disturbance, considers a permanent fault which needs to be isolated by the instantaneous trip operation of Bk 1. The second case study (Case 1.B), which represents a quite less severe disturbance than the prior case, assumes that the fault is temporary for a certain amount of time and implements an instantaneous trip action with automatic breaker reclosing at a preset delay-time of 250 ms prior to lock-out. A load shedding scheme (LS) is included in order to prevent the system frequency collapse during severe disturbances, but also to make use of the activated steps and consequently the rejected load as a performance comparison index for various scenarios including the STATCOM-SMES. This integrated controller is placed at bus 4 aiming at enhancing the dynamic security of the power system.

5.1.1. Case study 1.A: Large-signal performance analysis

The performance of the standard control of the power system, namely the base case without using any compensating device, is analyzed through the simulation results of Fig. 11, shown in black dashed lines. For the configuration presented in the test case prior to the fault in steady-state, the generator power production is 80 MW, and the active power demanded by the load is 120 MW so that the utility system needs to import about 40 MW from the bulk power system. In this interconnected operation, the system frequency is at its rated value (50 Hz) and the voltage at bus 4 is 1.01 p.u. After the fault is cleared and the tie-line tripped, the generator is operated in island conditions. Under these circumstances, the generator itself has to supply all the power required by the load. As can be seen from the simulation results, the spinning reserve of the unit is neither sufficiently large nor fast enough for supporting the system frequency through the PFC and thus avoiding the frequency drop which could cause the system collapse. The implementation of the automatic LS scheme with the activation of eight frequency steps (total load rejected of 40 MW/16 Mvar) is required in order to recover the system frequency to its scheduled value. Despite this fact, the generating unit must be able to ramp up very fast in order to decrease the amount of load rejected, and to ramp-down quickly for reducing the frequency deviation overshoot and settling time after the demand is stabilized, as can be derived from the mechanical power of the machine. Under these circumstances, the required demand cannot be fully satisfied bringing technical and economic consequences that are related to costs of deficits. After the fault clearance, a voltage overshoot of near 11.4% occurs until the voltage regulator of the unit stabilizes the bus voltage.

Consider now the inclusion at bus 4 of a standard ±80 Mvar STATCOM controller in the voltage control mode (VCM). The impact of the operation of this standard FACTS controller can be analyzed by simulation results of Fig. 11, shown in blue solid lines. The good performance of the voltage regulation at the PCC of the STATCOM is evidently depicted by the compensation of reactive power. The rapid exchange of reactive power after the fault clearance permits limiting the maximum voltage overshoot to near 7.5%, i.e. almost 3.9% lesser than the base case shown in dashed lines. PI controller gains of the external level control scheme in VCM were

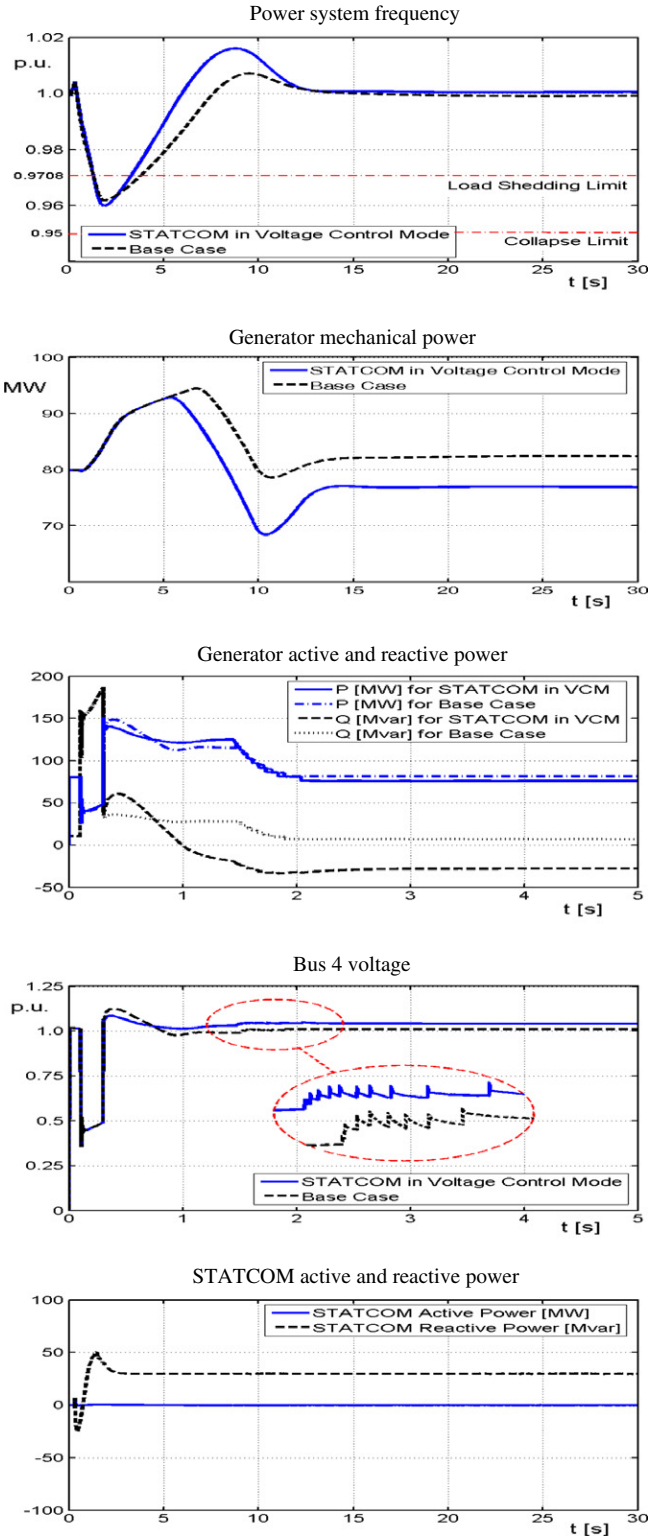

Fig. 11. Case study 1.A: Fault results for the base case and the case with a standard STATCOM in VCM.

determined to give the power system the fastest voltage regulation at bus 4 while keeping the maximum overshoot less than 10%. The shortest settling time obtained for this case study is 0.2 s, approximately 30% lesser than the base case. However, this control objective of the standard STATCOM device comes into conflict with the primary frequency control of the PS. Thus, by controlling the

voltage at bus 4, a larger active power flow is forced in the electric system which causes an increase of the system frequency drop and its rate of change after the disturbance. In this way, two extra frequency steps of load rejection needs to be activated respect to the base case (total 10 steps) in order to recuperate the system frequency during the disturbance effect. In the post-fault steady-state, the voltage level at bus 4 is enhanced by the STATCOM providing a compensation of approximately 30 Mvar, which allows increasing the voltage from 1.012 V in the base case to 1.043 V, representing a 3% improvement.

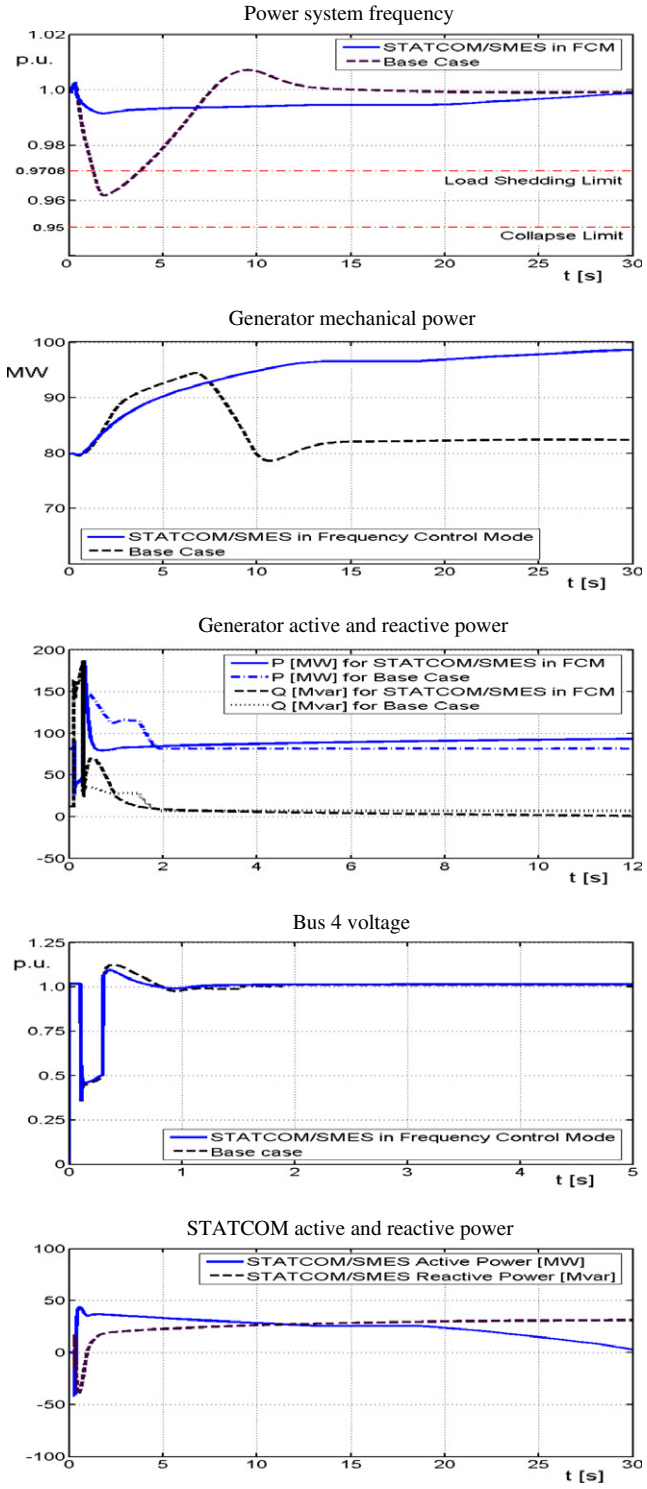

Fig. 12. Case study 1.A: Fault results for the for the base case and the case with an integrated STATCOM-SMES controller in FCM.

The effect of incorporating a 50 MW/800 MJ SMES coil into the dc bus of the conventional ±80 Mvar STATCOM device, yielding an enhanced integrated STATCOM-SMES controller, can be studied in the frequency control mode through the simulation results of Fig. 12, shown in blue solid lines. These results clearly show the outstanding dynamic performance of the FCM of the STATCOM-SMES. The rapid active power supply added to the conventional reactive power compensation, quickly absorbs the sudden power loss occurred after the tie-line tripping. Thus, the generator is able to find the balance with the load at a lower speed than in the previous test cases without producing a significant frequency deviation, resulting in a much smoother variation of the mechanical power of the machine. This condition permits to greatly decrease the power strain of the generating unit, which results in an improvement of the reliability of the power system. In this case, the effects of the disturbance are totally mitigated in a shorter time than in the base case without being necessary to activate the load shedding scheme. In fact, the frequency drop is drastically reduced and maintained far away from the load shedding limit. The minimum frequency reached during the disturbance is 0.9921 p.u. versus 0.9619 p.u. for the base case (shown in black dashed lines). Furthermore, the voltage profile at bus 4 is improved respect to the base case without requiring shedding load, showing a better performance than the standard voltage regulation of the generating machine, although the voltage profile obtained with SMES in FCM is somewhat worse than the STATCOM device in VCM. However, the SMES adds extra flexibility to the power system, allowing both objectives to be accomplished at the same time without rejecting load. The improvement of the PFC is obtained by the immediate action of the SMES coil for supplying/absorbing active power, which provides active power for about 30 s (approximately 735 MJ of energy). AGC control action has not been shown in order to focusing the study on the primary frequency control performance.

5.1.2. Case study 1.B: Small-signal performance analysis

The performance of the standard control of the power system (base case) is now analyzed for the case study 1.B, through the simulation results of Fig. 13, shown in black dashed lines. The disturbance occurring in the power system after the fault clearance and subsequent automatic reclosing of the breaker Bk1 causes electromechanical oscillations of the generator. These local oscillations, between the electrical machine and the rest of the electric system must be effectively damped to maintain the PS stability. During the fault period, the transfer of energy from the machines to the infinite bus is considerably reduced, and hence, the input mechanical energy during this period appears as an increase in the kinetic energy of the system with the consequent increase in the speed of the unit. Since the line resistances are inherently low, oscillations persist for a long time. As can be noted from digital simulations, a local mode of approximately 1.25 Hz that settles down to its steady state value only after 12 s is induced in the electric system. As expected, this low frequency power swing influences not only the system frequency, the rotor angle deviation and the active and reactive power supplied by the generating machine, but also the voltage profile at bus 4.

As in the previous case study, consider now the inclusion at bus 4 of a standard ±80 Mvar STATCOM operating in the VCM. The impact of incorporating this conventional FACTS controller can be studied by simulation results of Fig. 13, shown in blue solid lines. Although the objective of this control system mode is to support and regulate the voltage at the PCC of the STATCOM, which can be verified through the voltage profile at bus 4, the good performance of the voltage controller also succeeds to moderately damp

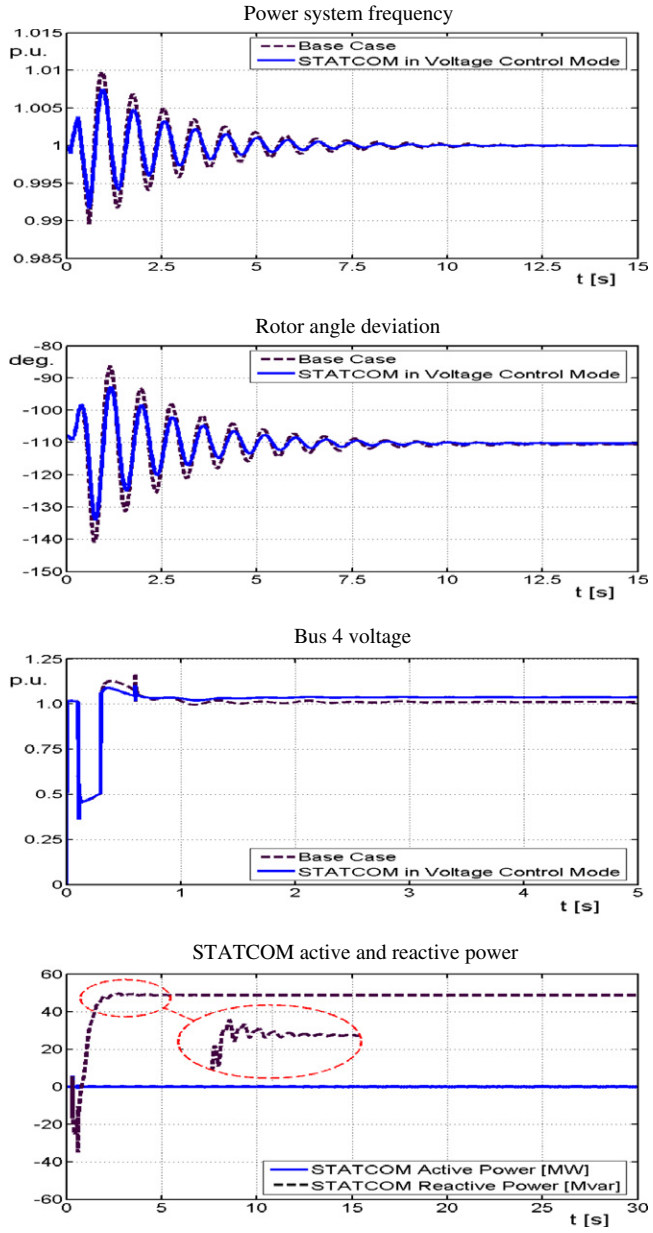

Fig. 13. Case study 1.B: Fault results for the base case and the case with a standard STATCOM in VCM.

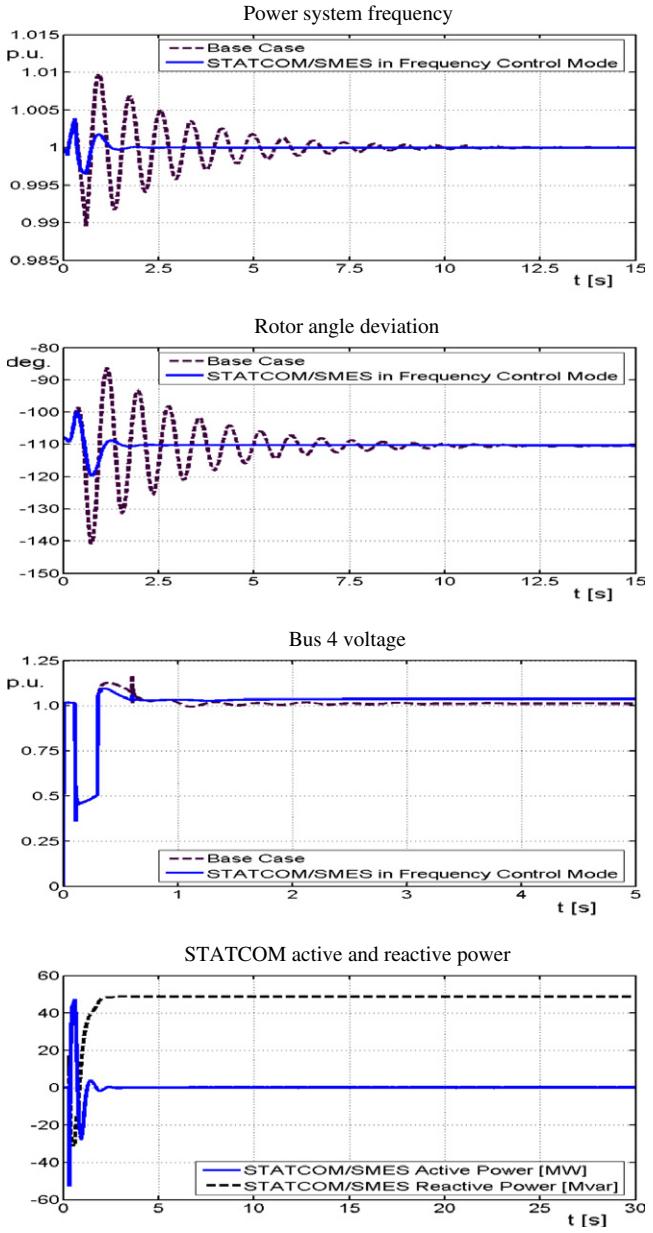

Fig. 14. Case study 1.B: Fault results for the for the base case and the case with an integrated STATCOM-SMES controller in FCM.

the low frequency oscillation mode. Aiming at controlling the voltage at bus 4, the compensation signal for voltage support (about 50 Mvar) also includes a superimposed oscillating component for stabilizing the voltage profile and thus reducing the amplitude of the oscillations.

The effect of incorporating a ±50 MW/800 MJ SMES coil into the dc bus of the conventional ±80 Mvar STATCOM can be verified through the simulation results of Fig. 14, shown in blue solid lines. The transient response clearly proves the outstanding small-signal dynamic performance of the frequency control mode of the STATCOM-SMES, the same as in the case for large signal studied. The SMES unit acts as an efficient damper, absorbing surplus energy from the system and releasing energy at the appropriate time when required. The SMES unit with the proposed controller is capable of damping the oscillations in a short time and reducing the amplitude of the pulsations on the frequency considerably. In the present analysis, the settling time for the system frequency is about 2 s when the SMES unit is used for active power compensation. This implies a reduction of almost 10 s respect to the base case. Furthermore, the frequency and rotor angle deviations are greatly reduced to values lesser than the maximum reached at the end of the fault when exists the peak increase in the kinetic energy of the system. A noteworthy point is that the capacity rating of the SMES unit used in this case study for damping low frequency power swings is only 6.3 MJ with a power rating of almost ±50 MW.

5.2. Case study 2: Simplified modeling evaluated in a real multi-machine test power system

The basic structure of the test power system used to study the dynamic performance of the STATCOM-SMES simplified models is presented in Fig. 15. This multi-machine network is a reduced model of the Argentinean high voltage (HV) interconnected system

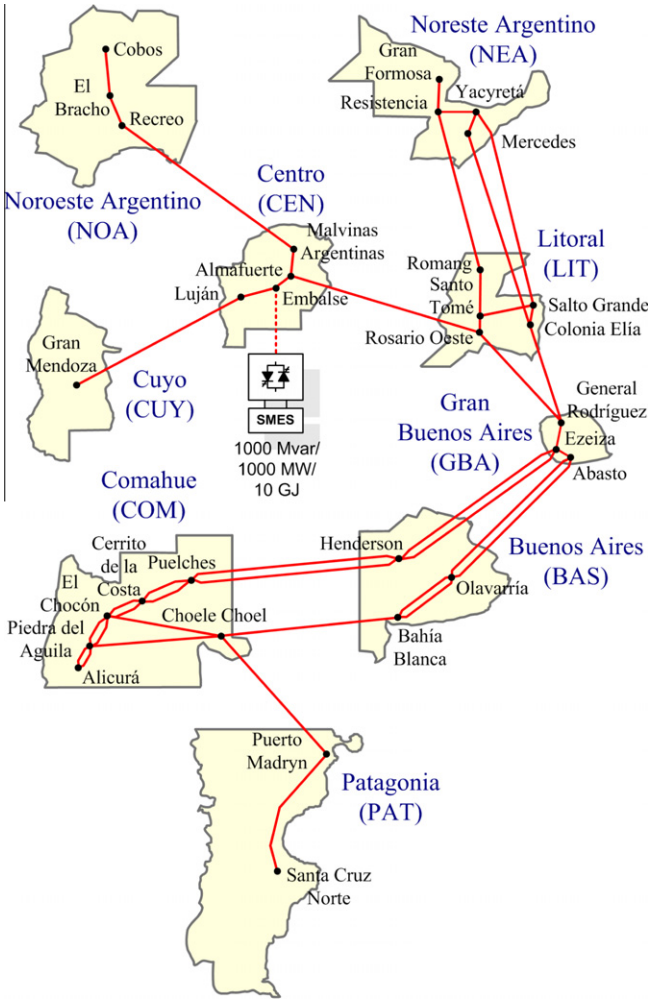

Fig. 15. Simplified model of the Argentinean high voltage interconnected system (or SADI).

(aka Sistema Argentino de Interconexión or SADI, in Spanish) [19]. The electricity sector in Argentina constitutes the third largest power market in Latin America, after Mexico and Brazil. This power sector is one of the most competitive and deregulated in South America, with unbundling in generation, transmission and distribution. Generation occurs in a competitive and mostly liberalized market in which 75% of the generation capacity is owned by private utilities. In contrast, the transmission and distribution sectors are highly regulated and much less competitive than generation. CAMMESA (Compañía Administradora del Mercado Mayorista Eléctrico, in Spanish) is the organization that schedules and supervises the electric system operation, i.e. the administrator of the Argentinean wholesale electricity market (Mercado Eléctrico Mayorista or MEM, in Spanish).

The Argentinean interconnected power system is modeled at 500 kV level as per December 2010 data [20], using an equivalent model build by identification of clusters of coherent machines. It is to be noted that all interconnections between some areas accomplished during 2011 were not consider in the proposed model. Once identified the clusters of coherent machines, the reduction of the size of the model is done by the creation of equivalent machines which substitute the set of original ones. This aggregation was done in such a way that all the machines in each cluster oscillate coherently in all the slowest modes of interest. This procedure is repeated for all areas, which in the proposed model are nine.

The main characteristics of the SADI power system are the following [19,20]:

- Group of nine electrical areas or clusters with different features of generation and demand.
- Hydro-Thermal structure with a peak demand of around 13,000 MW.
- Geographically extensive and unmeshed HV transmission system.
- Main low cost generation areas far from the major load centers, yielding high transmission losses.

The SADI is divided into nine regions or areas: *Cuyo* (CUY), *Comahue* (COM), *Noroeste Argentino* (NOA), *Centro* (CEN), *Buenos Aires* (BAS), *Gran Buenos Aires* (GBA), *Litoral* (LIT), *Noreste Argentino* (NEA) and *Patagonia* (PAT), as illustrated in Fig. 15. The most important generation areas are *Comahue* (COM) and *Noreste Argentino* (NEA) areas. In these areas, the generation is composed mainly of hydro power plants and, to a lesser extent, of thermal generation

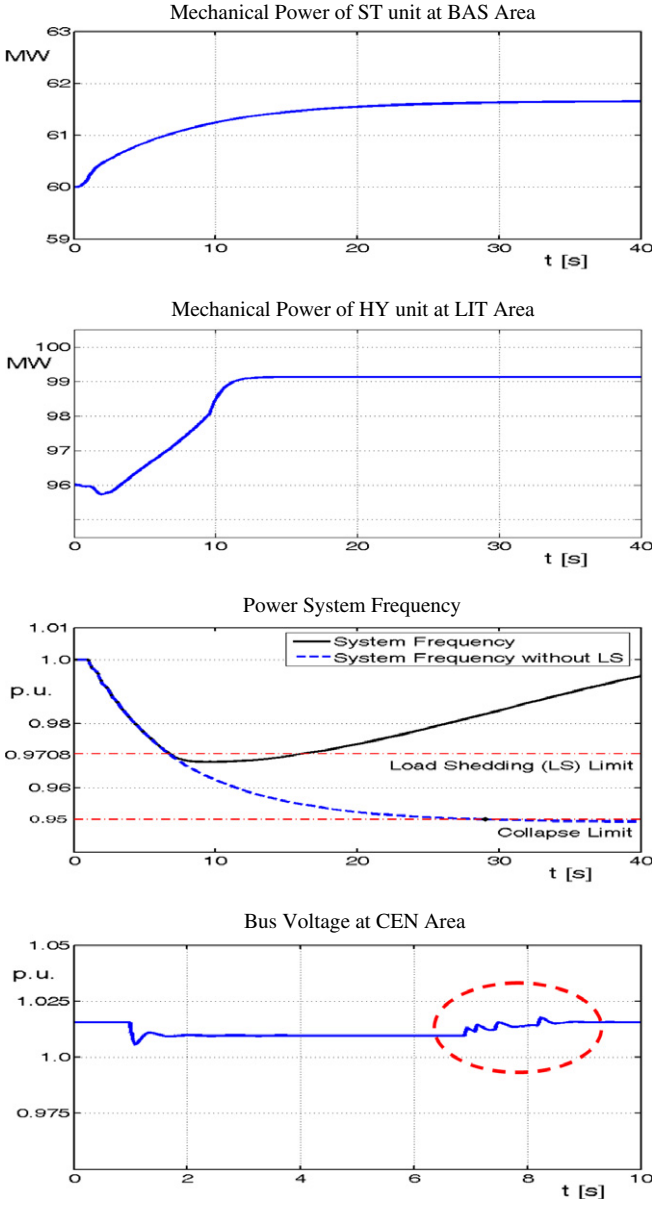

Fig. 16. Case study 2: Fault results for the base case (Conventional PFC).

units using low-cost natural gas. The main load centers are located in *Gran Buenos Aires* (GBA) and *Centro* (CEN) areas. Two transmission corridors of about 1100 km transport electric power from NEA and COM to GBA. The power grid consists of nine main nodes, including transformers and equivalent machines and 27 lines. Transient models are used for generators, including exciters, voltage regulators, power systems stabilizers and governors. Loads are represented as constant PQ and a load shedding scheme (LS) is implemented, activated by under-frequency and rate of change of frequency.

For the proposed dynamic studies, it is analyzed the condition of a sudden loss of the largest generation unit of the SADI. This scenario corresponds to the tripping of a 750 MW nuclear power plant in the CEN area, called *Embalse*, which represents almost the 10% of the generated power for the generation dispatch scenario considered of 7650 MW. These conditions are simulated by permanently opening the breaker which connects the generating unit to the corresponding bus, at $t = 1$ s. Due to the radial nature of the Argentinean network, the optimal location of the shunt FACTS-ESS for the proposed severe disturbance is in the same area of the perturbation. In this way, the proposed STATCOM-SMES system is placed in the CEN area aiming at enhancing the dynamic security of the electric system.

The performance of the conventional PFC, that is, the base case without using the STASTCOM-SMES is analyzed through the simulation results of Fig. 16. This case is used as a benchmark for all subsequent studies. As can be seen, the power system spinning reserve for PFC is insufficient to support the system frequency after the generation loss occurs (see frequency in blue dashed lines). For this reason, it is strongly necessary to activate the under-frequency LS to prevent a system frequency collapse (see frequency in black solid lines). The quantity of activated load shedding steps is used as a mitigation performance comparison index for various scenarios including the STATCOM-SMES system. In the base case studied, it is required the activation of four frequency steps in order to recover the system frequency and to avoid collapse. This corresponds to a total load shedding of almost 12%, equitably distributed on central and peripheral areas. Under these circumstances, the load shedding steps activated allows the generation reserve recovering the power system frequency. The generating units have to ramp up quickly to decrease the amount of load disconnected. This is shown through the mechanical power of a sample generator of BAS area (60 MW), representing the steam turbine (ST) plants response, and a sample generator of LIT area, representing the performance of the hydraulic (HY) turbine plants (96 MW). Disconnection of load also permits to improve the voltage profile at CEN area in each LS activation step. A brief overvoltage occurs until units' voltage regulators stabilize the bus voltage.

Consider now the inclusion at CEN area of an overall 1000 Mvar-1000 MW/10 GJ STATCOM-SMES system. The results of Fig. 17 clearly show the high effectiveness of the STATCOM-SMES system in the FCM. When the SMES system is activated as a consequence of the frequency deviation during the transient, a rapid active power supply is carried out. It allows to lessen the impact of the power system disturbance occurred; thus avoiding the activation of the load shedding scheme and recovering very quickly the system frequency. In this way, the injection of active power by the SMES system as well as the compensation of reactive power provided by the STATCOM permits to support the power system frequency for a sufficiently long period of time in order to allow the generating units which participate of the PFC to ramp up. This condition reduces the power strain on generators, especially for the faster units (HY) as seen on mechanical power output of Fig. 17. Even though the main objective of the STATCOM-SMES controller is the PFC and that during this action the voltage control is set to damp power oscillations, the voltage profile at CEN area is also greatly enhanced. Furthermore, the requirement of reactive power from generator units is reduced, which allows to increase the loading of transmission lines. The SMES system provides approximately 630 MW of maximum active power and 8950 MJ of energy in order to support the power system frequency, while the STATCOM generates 800 Mvar of maximum reactive power.

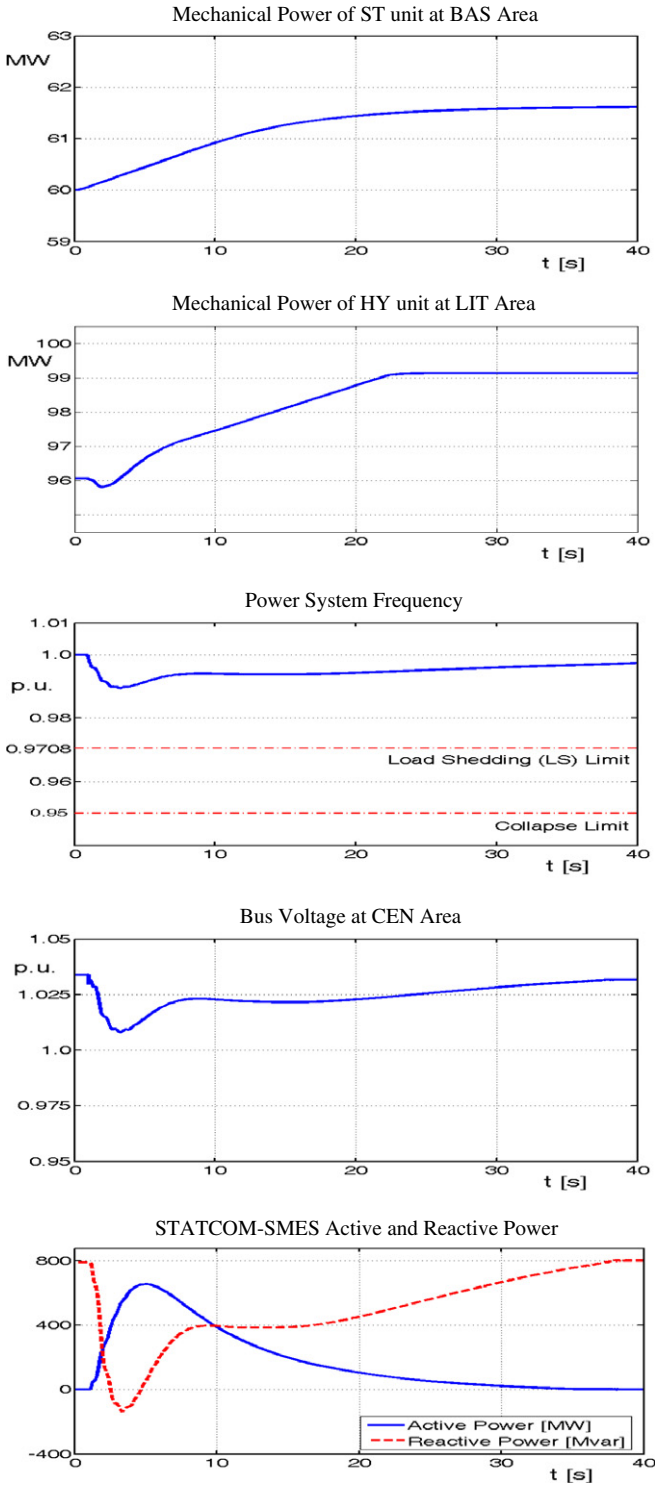

Fig. 17. Case study 2: Fault results for the for the base case and the case with an integrated STATCOM-SMES controller in FCM.

6. Conclusions

This paper presents a new concept of PFC based on incorporating a static converter-based shunt FACTS controller such as a Static Synchronous Compensator (STATCOM) coupled with a SMES system. A real detailed full model of the enhanced compensator and a novel control algorithm based on a decoupled current control strategy in the synchronous-rotating d–q reference frame are proposed. Moreover, a dynamic equivalent model of the proposed STATCOM-SMES for multi-machine power system studies is presented. The proposed simplified modeling is developed using the state-space averaging technique and is extended to an array of units through an aggregated model approach. Computer simulation results carried out in the MATLAB/Simulink environment using both discrete and phasor methods verify the effectiveness and robustness of the primary frequency control strategy proposed and the accuracy of models. The novel multi-level control scheme ensures fast controllability of the STATCOM-SMES operating in the four-quadrant modes, which enables to effectively increase the transient and dynamic stability of the power system, as well for small as for large-signal, in single and multi-machine electric power systems. The incorporation of the SMES system into the STATCOM also permits to reduce the requirement of spinning reserve of the electric system and the power strain of generators. The SMES with proposed novel control can efficiently act as a buffer between the PS and the disturbances arisen in the system.

Acknowledgments

This work was supported in part by the Argentinean National Agency for the Promotion of Science and Technology (ANPCyT) and the National University of San Juan (UNSJ) under Grant PICTO−UNSJ 2009, No. 0162.

References

[1] Deese AS, Nwankpa CO. Application of analog and hybrid computation methods to fast power system security studies. Int J Electr Power Energy Syst 2011;33(5):1140–50.
[2] Molina MG, Mercado PE, Watanabe EH. Static synchronous compensator with superconducting magnetic energy storage for high power utility applications. Energy Convers Manage 2007;48(8):2316–31.
[3] Dai1 Y, Zhao T, Tian Y, Gao L. Research on the influence of primary frequency control distribution on power system security and stability. Second IEEE conference on industrial electronics and applications (ICIEA); 2007. p. 222–6.
[4] Affonso CM, Da Silva LCP. Potential benefits of implementing load management to improve power system security. Int J Electr Power Energy Syst 2010;32(6):704–10.
[5] Karami A. Power system transient stability margin estimation using neural networks. Int J Electr Power Energy Syst 2011;33(4):983–91.
[6] Morison K. Power system security in the new market environment: future directions. IEEE PES Summer Meet 2002;3:1416–7.
[7] Gomes P. New strategies to improve bulk power system security: lessons learned from large blackouts. IEEE Power Energy Soc (PES) General Meet 2004;2:1703–8.
[8] Molina MG. Enhancement of power system security level using FACTS controllers and emerging energy storage technologies. In: Acosta MJ, editor. Advances in energy research, vol. 6. New York: Nova Science Publishers Inc.; 2011. p. 1–65.
[9] Ali MH, Wu B, Dougal RA. An overview of SMES applications in power and energy systems. IEEE Trans Sustain Energy 2010;1(1):38–47.
[10] Zhang XP, Rehtanz C, Pal B. Flexible AC transmission systems: modelling and control (Power Systems). 2nd ed. New York: Springer-Verlag; 2009.
[11] El-Moursi MS, Sharaf AM. Novel controllers for the 48-pulse VSC STATCOM and SSSC for voltage regulation and reactive power compensation. IEEE Trans Power Syst 2005;20(4):1985–97.
[12] Molina MG, Mercado PE, Watanabe EH. Improved superconducting magnetic energy storage (SMES) controller for high power utility applications. IEEE Trans Energy Convers 2011;26(2):444–56.
[13] Molina MG, Mercado PE, Watanabe EH. Analysis of integrated STATCOM-SMES based on three-phase three-level multi-pulse voltage source inverter for high power utility applications. Journal of the Franklin Institute 2011;348(9): 2350–77.
[14] Rodriguez J, Lai JS, Peng FZ. Multilevel inverters: a survey of topologies, controls, and applications. IEEE Trans Ind Electron 2002;49(4):724–38.
[15] Steurer M, Hribernik W. Frequency response characteristics of a 100 MJ SMES coil – measurements and model refinement. IEEE Trans Appl Superconduct 2005;15(2):1887–90.
[16] The MathWorks Inc. SimPowerSystems for use with Simulink: user's guide; 2011. <www.mathworks.com>.
[17] Singh B, Jayaprakash P, Kothari DP. New control approach for capacitor supported DSTATCOM in three-phase four wire distribution system under non-ideal supply voltage conditions based on synchronous reference frame theory. Int J Electr Power Energy Syst 2011;33(5):1109–17.
[18] Molina MG, Mercado PE. Power flow stabilization and control of microgrid with wind generation by superconducting magnetic energy storage. IEEE Trans Power Electron 2011;26(3):910–22.
[19] Del Rosso A, Cañizares CA, Quintana V, Doña V. Stability improvement using TCSC in radial power systems. NAPS; 2000. p. 1–8.
[20] CAMMESA (Compañía Administradora del Mercado Mayorista Eléctrico, the administrator of the Argentinean wholesale electricity market). Argentinean high voltage interconnected system (SADI in Spanish) data; 2011. <http://www.cammesa.com>.